RESEARCH ARTICLE | MARCH 26 2025

Blocking phenomenon induced by droplet electrocoalescence and wavy walls

Yuan Ma (马原); Rasul Mohebbi ; Zhigang Yang (杨志刚)

Physics of Fluids 37, 033629 (2025)
https://doi.org/10.1063/5.0263873

Physics of Fluids ARTICLE pubs.aip.org/aip/pof

Blocking phenomenon induced by droplet electrocoalescence and wavy walls

Cite as: Phys. Fluids **37**, 033629 (2025); doi: 10.1063/5.0263873
Submitted: 7 February 2025 · Accepted: 8 March 2025 ·
Published Online: 26 March 2025

Yuan Ma (马原),[1] Rasul Mohebbi,[2,a)] and Zhigang Yang (杨志刚)[3,4,5]

AFFILIATIONS

[1]Department of Civil and Environmental Engineering, The Hong Kong Polytechnic University, Hong Kong SAR, People's Republic of China
[2]School of Engineering, Damghan University, P.O. Box: 3671641167, Damghan, Iran
[3]School of Automotive Studies, Tongji University, Shanghai 201804, People's Republic of China
[4]Shanghai Automotive Wind Tunnel Center, Tongji University, Shanghai 201804, People's Republic of China
[5]Beijing Aeronautical Science & Technology Research Institute, Beijing 102211, People's Republic of China

[a)]Author to whom correspondence should be addressed: rasul_mohebbi@du.ac.ir

ABSTRACT

This study explores the impact of wavy walls and electric fields on the deformation and coalescence of droplets using a fully coupled model developed in COMSOL. The model integrates the Navier–Stokes equations, Maxwell stress tensor, and phase-field model to analyze the effects of electric field strength, wavy wall amplitude, and wavy wall wavelength. It can be found that in a cavity with flat walls and no applied electric field, droplets coalesce and descend. At low electric field strengths, droplets adhere to one sidewall, altering their descent. With an increased potential of 2000 V, droplets coalesce to form a stationary barrier layer that divides the cavity into upper and lower sections. The presence of wavy walls significantly influences droplet behavior. At $A = 0.5$, $L = 5$, and $V_0 = 2000$ V, an inclined barrier layer form. Increasing the A enhances the influence of the wavy walls, thereby decelerating the descent of the droplets. Conversely, reduced L inhibits droplet descent. This study highlights the complex interplay between electric fields and wavy walls in controlling droplet dynamics.

NOMENCLATURE

A	Amplitude
$\boldsymbol{D}$	Electric displacement
$\boldsymbol{E}$	Electric field
$\boldsymbol{F_E}$	Electric body force
$\boldsymbol{F_{st}}$	Surface tension force
$\boldsymbol{I}$	Identity tensor
$\boldsymbol{g}$	Gravitational acceleration
H	Height
L	Wavelength
p	Pressure
$\boldsymbol{T}$	Maxwell stress tensor
$\boldsymbol{u}$	Velocity
V_0	Electric potential
W	Width
χ	Interfacial mobility adjustment parameter
μ	Dynamic viscosity
ρ	Density
σ	Surface tension coefficient
ϵ	A parameter related to the interface thickness
ϕ	Phase-field variable

I. INTRODUCTION

The coalescence phenomenon refers to the physical interaction between two miscible droplets, which can be of the same or different phases, surrounded by another fluid.[1–3] It is attracting increasing research interest due to its critical role in fundamental fluid dynamics,[4] heat transfer,[5] environmental management,[6] advanced materials,[7] energy applications,[8] and biological systems.[9]

To precisely control the timing and location of droplet coalescence, the process can be facilitated by applying external energy or forces. These external stimulations can include magnetic fields,[10] acoustic waves,[11] or electric fields.[12] Ghaffari *et al.*[13] conducted Computational Fluid Dynamics (CFD) simulations to investigate the deformation and coalescence dynamics of ferrofluid droplets subjected to a uniform magnetic field. Their findings revealed that the

application of a magnetic field to the ferrofluid droplets induced an attractive force between the droplets, facilitating their approach toward each other. Hassan *et al.*[14] conducted a numerical investigation on the interaction of two droplets under a uniform magnetic field, where the droplets differed in size. Their findings indicated that when a magnetic field was applied along the horizontal direction, the droplets formed round-bottom hull-shaped configurations. Conversely, under a vertical magnetic field, the droplets transformed into teardrop-shaped configurations prior to coalescence.

In addition to magnetic fields, acoustic waves can also influence the coalescence dynamics of droplets. Taleghani and Noori[15] studied the effect of surface acoustic waves on two same droplets coalescence phenomena. Under the influence of acoustic waves, the dynamics of droplets change, overcoming the coalescence phenomenon, and minimizing surface energy becomes challenging, leading to an increase in coalescence time. Adeyemi *et al.*[16] conducted numerical simulations to investigate water droplet coalescence in crude oil under the influence of ultrasound waves. They observed that an increase in droplet size led to a delay in the restoration of the droplets to their spherical forms after initial deformation, as the Weber number increased.

Electrocoalescence technology is extensively utilized in two-phase separation due to its high efficiency, cost-effectiveness, and environmental benefits. Huang *et al.*[17] conducted an investigation on the deformation and coalescence behaviors of water droplets in a viscous fluid by applying a direct current electric field. Their findings indicate that the temporal evolution of the liquid bridge is primarily governed by the interfacial tension and the viscosity of the continuous phase. Mardani *et al.*[18] numerically studied the coalescence of saltwater droplets in crude oil under a uniform electric field. They found that when the fluid velocity decreases or the electric field intensity increases, the time required for droplet coalescence decreases. Li *et al.*[19] conducted a numerical study on the transformation of drop-interface electrocoalescence modes under direct current electric fields. The drop-interface electrocoalescence process involves a competition between electrostatic stress and interfacial tension, which is determined by the coupling effects of electrical and physical parameters.

The distribution of the electric field significantly affects droplet coalescence. Therefore, it is essential to properly arrange the electric field during the electrocoalescence process. Luo *et al.*[20] conducted an experimental study on the evolution of water droplets within an oil phase under various electric field configurations. Their findings indicate that non-uniform electric fields significantly improve the efficiency of electrocoalescence compared to uniform electric fields. Hadidi *et al.*[21] numerically investigated electrocoalescence utilizing CFD methods. They explored the effect of a concentric semi-elliptic non-uniform electric field. They revealed that the shape of the applied non-uniform fields can significantly affect electrocoalescence performance in complex ways, which are sensitive to the drop-medium system. The effect of pulsatile electric field has been studied by Mousavi *et al.*[22] By applying various electric fields, they observed outcomes including complete coalescence, partial coalescence, and rebound without coalescence. Additionally, they found that the secondary droplets produced at very low-frequency pulsatile or direct current electric fields can be suppressed by increasing the frequency of the pulsatile electric field. Sun *et al.*[23] conducted an experiment to investigate the behavior of droplets falling and coalescing under alternating electric fields. They observed that falling droplets oscillated in both shape and trajectory when subjected to an electric field. Additionally, they found that increasing the electrical frequency reduced the degree of droplet deformation and extended the time required for the droplets to reach the interface.

According to the authors' knowledge, research on the effects of non-uniform electric fields on droplet coalescence is extremely limited. Despite the established fact that non-uniform electric fields outperform uniform electric fields, there still exists a significant gap in this field. More specifically, as of now, there is still no comprehensive understanding of the exact impact of the shape of the electric field medium on the coalescence time of droplets. The current work primarily investigates the influence of a non-uniform electric field on droplet coalescence. For the first time, the deformation and coalescence process of two freely falling water droplets in a wavy wall and the effects of electric field strength, amplitude, and length of wavy wall are studied.

This study offers critical insights into the behavior of droplets under the influence of electric fields and wavy wall geometries, with significant implications for various practical applications. These findings are particularly pertinent to the design and optimization of microfluidic devices, where the precise control of droplet dynamics is essential. This includes applications such as lab-on-a-chip technologies, where the effective manipulation and separation of droplets is of paramount importance. Moreover, the outcomes of this research have broader applications in fields such as inkjet printing and emulsion stabilization, where a deep understanding of the interaction between droplets and external fields can lead to improvements in product quality and process efficiency. In the context of oil–water separation and related industrial processes, our findings may inform the development of more effective strategies for controlling and managing droplet formation and behavior.

II. PHYSICAL MODEL AND METHOD

A. Physical model

Figure 1 illustrates the geometric schematic and boundary conditions used in the current study. The upper and lower walls of the medium are flat walls, while the left and right walls are symmetrical wavy walls. The walls of the cavity are all non-slip surfaces. An electrode with an electric potential of V_0 is positioned on the left wavy surface, while the right wavy surface is grounded. The cavity is filled with fluid, and there are two droplets of a different fluid located at the upper interior of the cavity. In this study, W represents the width of the channel, while H denotes the height of the channel. It is noteworthy that, in the present study, while the shapes of the curved wall surfaces on both the left and right sides are altered, the value of W remains constant. D is the initial diameter of the two droplets. The parameters A and L control the sinusoidal waviness of the sidewalls of the channel, where L is the wavelength of the sinusoidal surface and A is the amplitude of the waviness. It is important to note that, in addition to the electric potential, the effects of the parameters A and L are also investigated. Accordingly, the values for the amplitude of the wavy wall are $A = 0$, 0.25, 0.5, and 0.75, while L, the wavelength of the wavy wall, is set to $L = 0$, 2.5, 5, and 7.5. The functions of the left and right wall surfaces of the cavity are represented by the following equations:

$$x = -A \sin \frac{2\pi}{L} y, \tag{1}$$

$$x = A \sin \frac{2\pi}{L} y + W. \tag{2}$$

In the current study, the base fluid within the cavity is oil, while the droplets are composed of water. Table I illustrates the properties of these two liquids.

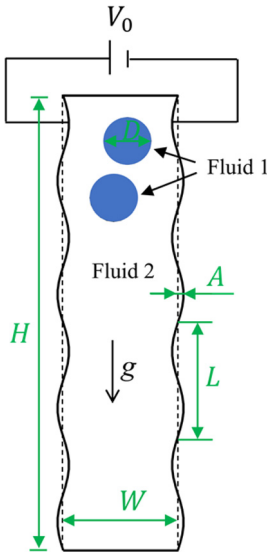

FIG. 1. Schematic representation of two uniform-sized droplets in a rectangular cavity with an applied electric field. The green labels in the figure denote length. The potential difference between the left and right walls of the cavity is V_0. The direction of gravity is vertically downward.

B. Governing equations

This section presents the governing equations for the electrohydrodynamic (EHD) of droplet coalescence in a two-phase system. These equations integrate the dynamics of fluid flow, electric fields, and interfacial phenomena. EHD encompasses the study of fluid motion influenced by electric fields.

The continuity equation for an incompressible fluid is given by

$$\nabla \cdot \boldsymbol{u} = 0, \tag{3}$$

where $\boldsymbol{u}$ is the fluid velocity. The momentum conservation in the fluid is described by the Navier–Stokes equation,

$$\frac{\partial \boldsymbol{u}}{\partial t} + \rho(\boldsymbol{u}\cdot\nabla)\boldsymbol{u} = \nabla\cdot\left[-p\boldsymbol{I} + \mu\left(\nabla\boldsymbol{u} + (\nabla\boldsymbol{u})^T\right)\right] + \rho\boldsymbol{g} + \boldsymbol{F}_{st} + \boldsymbol{F}_E. \tag{4}$$

Here, ρ is the fluid density, p is the pressure, $\boldsymbol{I}$ is the identity tensor, μ is the dynamic viscosity, $\boldsymbol{g}$ is the gravitational acceleration, $\boldsymbol{F}_{st}$ represents the surface tension force, and $\boldsymbol{F}_E$ denotes the electric body force.

The phase-field equations can simulate complex interfacial behaviors, with the evolution of phase-field variables governed by the following equations:

$$\frac{\partial \phi}{\partial t} + \boldsymbol{u}\cdot\nabla\phi = \nabla\cdot\frac{3\chi\sigma\epsilon}{2\sqrt{2}}\nabla\psi, \tag{5}$$

$$\psi = -\nabla\cdot\varepsilon^2\nabla\phi + \left(\phi^2-1\right)\phi, \tag{6}$$

where χ is the interfacial mobility adjustment parameter, σ is the surface tension coefficient, ϵ is a parameter related to the interface thickness, and ø is the phase-field variable.

The volume fractions of fluid 1 and fluid 2 were computed using the phase-field variable ϕ,

$$\Lambda_{f2} = \min\left(\max\left(\left[\frac{(1+\phi)}{2}\right], 0\right), 1\right), \tag{7}$$

$$\Lambda_{f1} = 1 - \Lambda_{f2}. \tag{8}$$

The effective density and viscosity of the interface are given by

$$\rho = \rho_1 + [\rho_2 - \rho_1]\Lambda_{f2}, \tag{9}$$

$$\mu = \mu_1 + [\mu_2 - \mu_1]\Lambda_{f2}, \tag{10}$$

where $\rho 1$, $\rho 2$, $\mu 1$, and $\mu 2$ are the densities and viscosities of the two phases.

The surface tension force in Eq. (2) is given by

$$\boldsymbol{F}_{st} = G\nabla\phi, \tag{11}$$

$$G = \lambda\left(-\nabla^2\phi + \frac{\phi\left(\phi^2-1\right)}{\epsilon^2}\right), \tag{12}$$

$$\lambda = \frac{3\sigma\epsilon}{2\sqrt{2}}. \tag{13}$$

The electric body force in Eq. (2) is computed as

$$\boldsymbol{F}_E = -\nabla\cdot T, \tag{14}$$

where $\boldsymbol{T}$ is the Maxwell stress tensor

$$\boldsymbol{T} = \boldsymbol{E}\boldsymbol{D}^T - \frac{1}{2}(E\cdot D)\boldsymbol{I}, \tag{15}$$

and $\boldsymbol{E}$ is the electric field

$$\boldsymbol{E} = -\nabla V, \tag{16}$$

with the electric displacement $\boldsymbol{D}$ given by[18,24]

$$\boldsymbol{D} = \varepsilon_0\varepsilon_r\boldsymbol{E}, \tag{17}$$

satisfying

$$\nabla\cdot(\varepsilon_0\varepsilon_r\nabla V) = 0, \tag{18}$$

where ε_0 is the vacuum permittivity and ε_r is the relative permittivity. The relative permittivity for each fluid was obtained by the internally defined volume fractions of each fluid,

TABLE I. The parameters of the liquids in the present work.

Liquids	Conductivity ($\mu s\cdot m^{-1}$)	Density ($kg\cdot m^{-3}$)	Viscosity (mPa·s)	Dielectric constant
Water	5.49	1000	1.0	80.0
Sunflower oil	7.62×10^{-5}	922	46.5	4.9

TABLE II. Physical parameters used for the verifications[27].

Case No.	$\rho 1$ (kg/m^3)	$\rho 2$ (kg/m^3)	$\mu 1$ (Pa·s)	$\mu 2$ (Pa·s)	σ (N/m)
1	1000	10	10	1	24.5
2	1000	1	10	0.1	1.96

$$\varepsilon_r = \varepsilon_{r1}\Lambda_{f1} + \varepsilon_{r2}\Lambda_{f2}. \tag{19}$$

The Maxwell stress tensor is defined by

$$T = \begin{pmatrix} T_{xx} & T_{xy} \\ T_{yx} & T_{yy} \end{pmatrix} = \begin{pmatrix} \varepsilon_0\varepsilon_r E_x^2 - \frac{1}{2}\varepsilon_0\varepsilon_r\left(E_x^2 + E_y^2\right) & \varepsilon_0\varepsilon_r E_x E_y \\ \varepsilon_0\varepsilon_r E_y E_x & \varepsilon_0\varepsilon_r E_y^2 - \frac{1}{2}\varepsilon_0\varepsilon_r\left(E_x^2 + E_y^2\right) \end{pmatrix}. \tag{20}$$

C. Solution procedure

The governing equations are solved by the finite element method based COMSOL Multiphysics software. For the coalescence dynamics of two droplets surrounded by a different fluid, the two-phase level-set method is used. This is a powerful software that provides scholars with the capability to simultaneously simulate different physical characteristics of a problem.[25,26]

III. VERIFICATION AND GRID SENSITIVITY ANALYSIS

Before commencing the present simulations, the accuracy of the numerical solver must be validated to ensure its reliability. To achieve this, various test cases were computed and compared with results from previous studies. The first verification involves the surface dynamics of a freely rising bubble. For this problem, two different fluid systems were validated. Table II presents the physical parameters of the two fluid systems, namely case 1 and case 2.

Figure 2 shows a comparison between the current computational results for case 1 and the results from Klostermann *et al.*[27] and Sormoli *et al.*[28] It can be observed that in case 1, where surface tension is dominant, the bubble deformation during ascent is not very significant. Figure 3 presents the comparison results for case 2. In this case, the density ratio and viscosity ratio are higher, and the influence of surface tension is relatively smaller. As a result, the bubble undergoes more significant deformation during its ascent. Through comparison, it can be observed that the computational results demonstrate perfect agreement.

The second verification case examines the coalescence behavior of two droplets under the influence of an electric field. Figure 4 shows a comparison between the current results and those of Sun *et al.*[24] at different time. The applied electric potential is 8000 V. The current comparison results demonstrate good consistency.

For the investigation of grid independence, the computational results were obtained for six different mesh schemes: Mesh 1 (2654), Mesh 2 (5492), Mesh 3 (8916), Mesh 4 (13812), Mesh 5 (59946), and Mesh 6 (219940). Figure 5 illustrates the voltage profiles along the axis at $t = 0.4$s for these different grid resolutions. It can be observed that the curves of the computational results corresponding to Mesh 5 and Mesh 6 almost overlap. Therefore, the current simulations utilize the mesh scheme of Mesh 5.

IV. RESULTS AND DISCUSSION

This section comprehensively presents the results of this study. The effects of the applied electric field intensity ($V_0 = 0$, 500, 1000, 2000), wavy wall amplitude ($A = 0$, 0.25, 0.5, 0.75), and wavy wall wavelength ($L = 0$, 2.5, 5, 7.5) on the coalescence phenomenon between two droplets are thoroughly investigated. In this section, the process of electrocoalescence of droplets within the cavity is illustrated through various representations, including droplet phase diagrams, electric potential contours, force distribution, streamlines, electric potential curves, and velocity profiles.

A. Impact of electric force with flat walls

Figure 6 illustrates the potential distribution and the motion of the droplets in the case with flat walls for different V_0. When no electric field is applied ($V_0 = 0$), the droplets, being very close to each other, will quickly coalesce and gradually form a circular shape. At $t = 0.03$s, the two droplets have already coalesced. Due to the influence of gravity, the coalesced droplet descends within the cavity. When V_0 increases to 500 V, the voltage is relatively low, so the influence of electric field on the droplets is not significant. The curve depicted in the

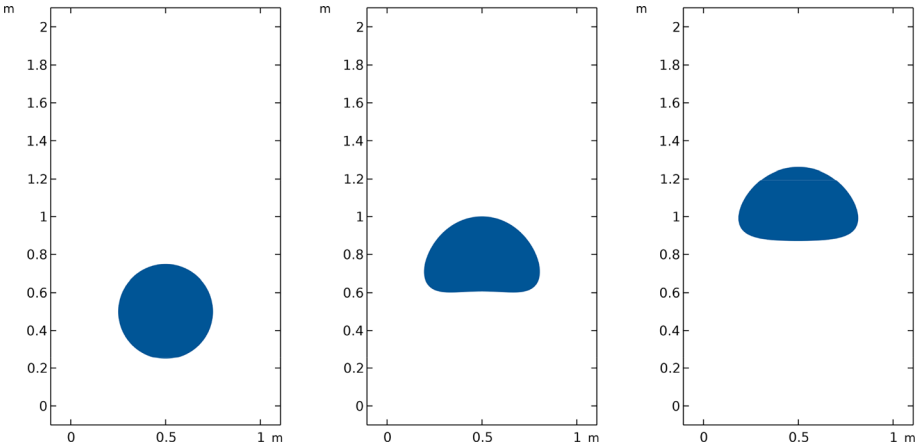

FIG. 2. Case 1: the evolution of bubble shape over time (from left to right: 0 s, 1.5 s, 3 s). The above figures, obtained from present solver, are compared with the results from Klostermann *et al.*[27] and Sormoli *et al.*[28]

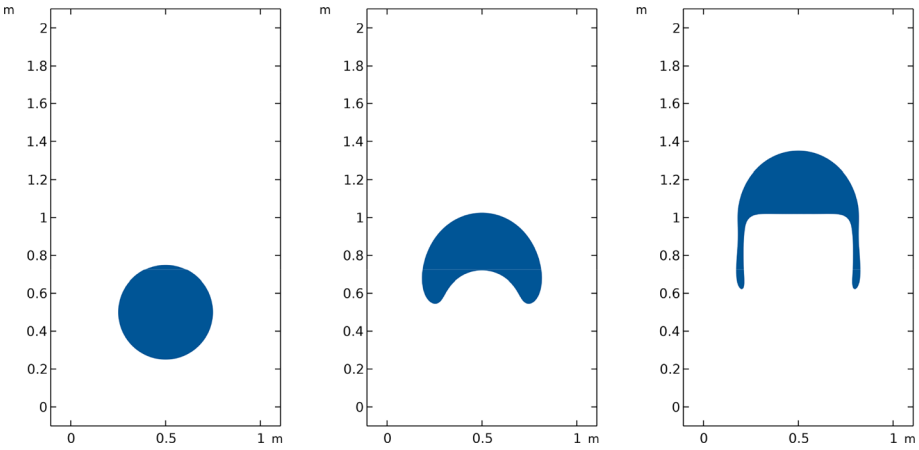

FIG. 3. Case 2: the evolution of bubble shape over time (from left to right: 0 s, 1.5 s, 3 s). The present solver is validated by comparing the above figures with the results from by Klostermann *et al.*[27] and Sormoli *et al.*[28]

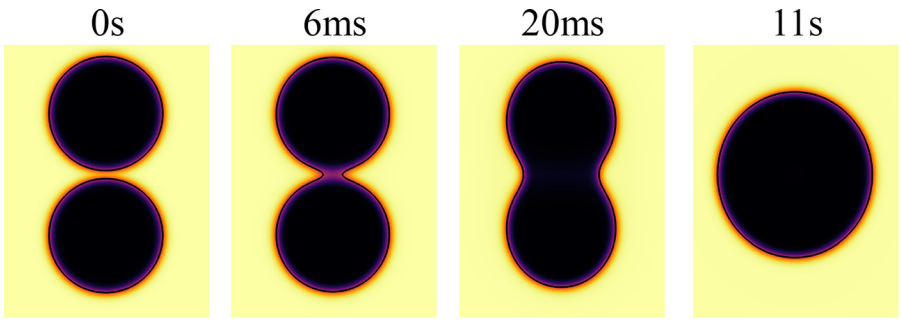

FIG. 4. Electrocoalescence behavior between drops under varying electric field parameters at $V_0 = 8000$ V. The above figures from the present solver are validated against the results of the experimental work by Sun *et al.*[24]

figure represents the equipotential lines of electric potential. For the sake of comparison, the local electric potential V has been normalized using V_0, resulting in equipotential lines that illustrate the ratio of the local electric potential to V_0. The subsequent contour maps of electric potential will utilize the same type of equipotential lines (V/V_0), and further elaboration on this methodology will not be reiterated. Nevertheless, a comparison reveals that at $t = 10$ s, the droplets with $V_0 = 500$ V are closer to the wall compared to those with $V_0 = 0$. It can be observed that the electric potential gradient between the sides of the droplet and the side walls is significantly greater than the electric potential gradient within the droplet itself. When V_0 increases to 2000 V, the influence of the electric field on the droplets becomes very significant. Due to the influence of the horizontal electric field, the droplet experiences a horizontal tensile force, which can be seen in Fig. 7. Compared to the cases with lower V_0 or no electric field, at $t = 0.03$s, the droplets still have not coalesced, with coalescence occurring at $t = 0.04$s. On the other hand, at $t = 4$s, the coalesced droplet forms a barrier layer that divides the cavity into upper and lower sections. Notably, similar barrier layers are utilized in embolization procedures to inhibit the growth of tumor cells.[29] Moreover, as time progresses, this barrier layer does not descend.

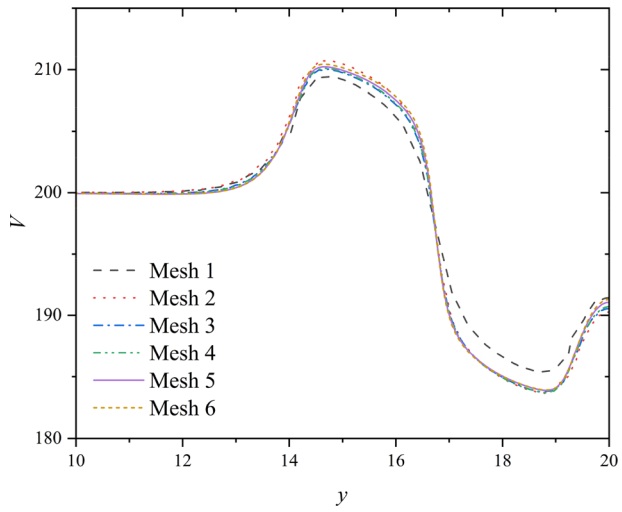

FIG. 5. The distribution curve of electric potential along the central axis at $t = 0.4$s for different mesh schemes: Mesh 1 (2654), Mesh 2 (5492), Mesh 3 (8916), Mesh 4 (13812), Mesh 5 (59946), and Mesh 6 (219940).

Figure 8(a) illustrates the schematic of the y-coordinate system used in Fig. 8(b). It is important to note that the y-coordinate employed in the subsequent sections remains consistent with the one outlined here. Therefore, further elaboration on this will not be provided. At $t = 0.01$s, a sinusoidal-shaped curve forms near $y = 16$. As time progresses to $t = 0.03$s, the sinusoidal shape persists, but the amplitude of the curve decreases significantly. Notably, at $t = 10$s, the voltage along the central axis stabilizes at 1000 V across different values of y.

Figure 9 presents the streamlines and velocity contour plots of the cavity at various moments for the case with flat walls at

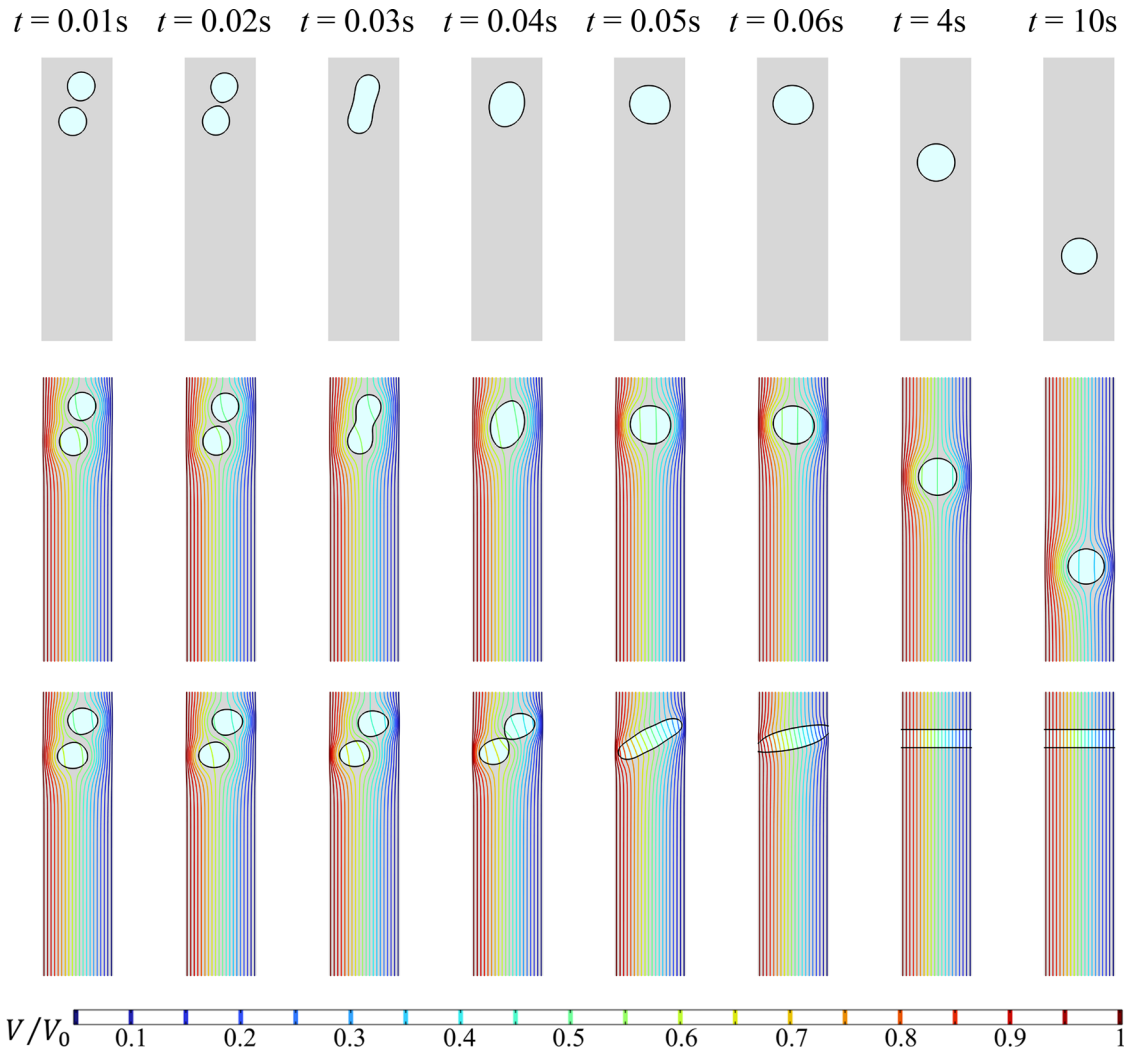

FIG. 6. Electric potential distribution and the motion of the droplets in the case with flat walls for different V_0: first row: $V_0 = 0$; second row: $V_0 = 500$ V; third row: $V_0 = 2000$ V. The contour lines represent the relative electric potential, which is the ratio of the local electric potential to V_0.

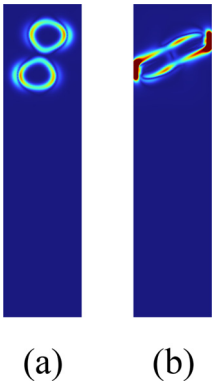

FIG. 7. Distribution of force of the case with flat walls at $V_0 = 2000$ V for different moments: (a) $t = 0.01$s; (b) $t = 0.05$s.

$V_0 = 2000$ V. It can be observed that during the electro-coalescence of the droplets, the movement and coalescence of the droplets induce fluid motion, resulting in higher velocities near the droplets. However, once the droplets form a stable barrier layer, both the droplets and the fluid remain nearly stationary under the influence of the electric field, leading to very low velocities. This behavior is evident in the streamlines and velocity contour plots within the cavity at $t = 4$s and $t = 10$s.

To provide a clearer comparative analysis of the barrier layer formed under high voltage, the velocity curves at $t = 10$s were compared. Figure 10 shows the velocity curve in the y-direction (U_y) along the central axis for the case with flat walls for different electric field strength. It can be observed that at $t = 10$s, the fluid is still in motion when $V_0 = 0$ or 500 V. However, when V_0 is set to 2000 V, a stable barrier layer forms, resulting in near-zero velocity.

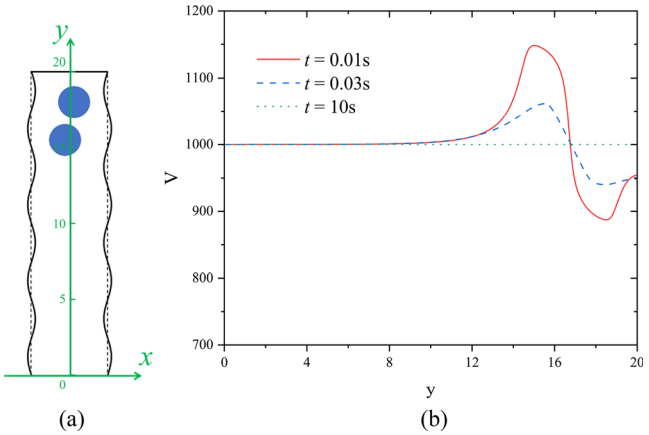

FIG. 8. (a) The coordinate schematic. (b) Electric potential curve along the center axis in the case with flat walls at $V_0 = 2000$ V. The coordinates in Fig. 8(b) are labeled as indicated in Fig. 8(a).

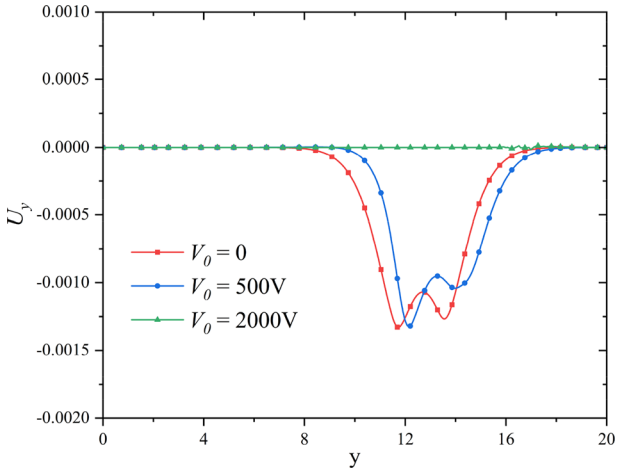

FIG. 10. Velocity curve in the y-direction along the center axis in the case with flat walls at $t = 10$s.

B. Curved walls

In the current section, the dynamics of droplet coalescence under the influence of an electric field in a cavity with wavy walls are investigated. Figure 11 shows the electric potential distribution and the motion of the droplets at $A = 0.5$ and $L = 5$ for different V_0. In the absence of an applied electric field, the variations in the wall boundaries have minimal impact on the coalescence of the droplets. Comparing with Fig. 6, it can be observed that when $V_0 = 0$, the shape and position of the droplets in the cavities with flat walls and wavy walls are nearly identical. Significant changes occur when the shape of side walls changes from flat to wavy. Notably, since the side walls serve as electrodes, alterations in their shape also lead to changes in the electric field distribution. For the cavity with wavy walls at $V_0 = 500$ V, after the droplets coalesce, it can be observed at $t = 4$s that the droplets have already been pulled toward the right-sidewall. By $t = 10$s, due to the coupling effect of the electric field and the side walls, the droplets do not descend. When V_0 is increased to 2000 V, a barrier layer still forms. However, compared to the flat wall cavity, the current partition layer is inclined.

Figure 12 shows the electric potential curve along the center axis for the case with $A = 0.5$ and $L = 5$ at $V_0 = 2000$ V. By comparing with Fig. 8, it can be observed that the electric potential curves are similar. However, it is noteworthy that at $t = 10$s, the electric potential curve is not a straight line, which is due to the inclined nature of the formed barrier layer.

Figure 13 illustrates the streamlines and velocity contour plot for the case with $A = 0.5$ and $L = 5$ at $V_0 = 2000$ V. Although there are differences in the shape of side walls, the mechanism by which the droplets coalesce and are stretched to form a barrier layer under the influence of the strong electric field remains largely unchanged. By $t = 4$s and $t = 10$s, the barrier layer has already formed, and the fluid is nearly stationary.

C. Effect of A

Based on the above analysis, it is evident that the coupling effect of wall shape and electric field significantly influences the movement and coalescence of droplets. Therefore, in the following sections, the phenomenon of droplet electro-coalescence will be considered under different geometric parameters (A and L) of the wavy walls. Figure 14 presents the droplet shape, position, and electric potential distribution at $V_0 = 500$ V, $t = 10$s, and $L = 5$ for different wavy wall amplitudes. It is worth noting that when $A = 0$, the side walls are flat. Comparing with Figs. 6 and 11, it can be observed that as A increases, the

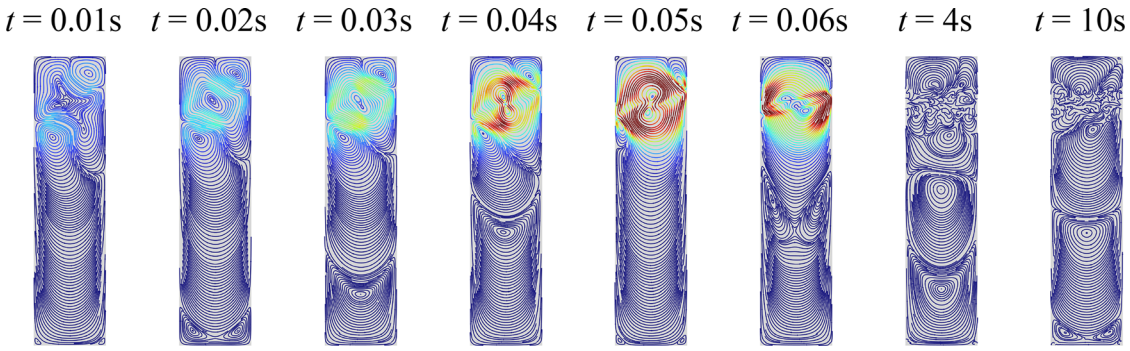

FIG. 9. Streamlines of the case with flat walls at $V_0 = 2000$ V.

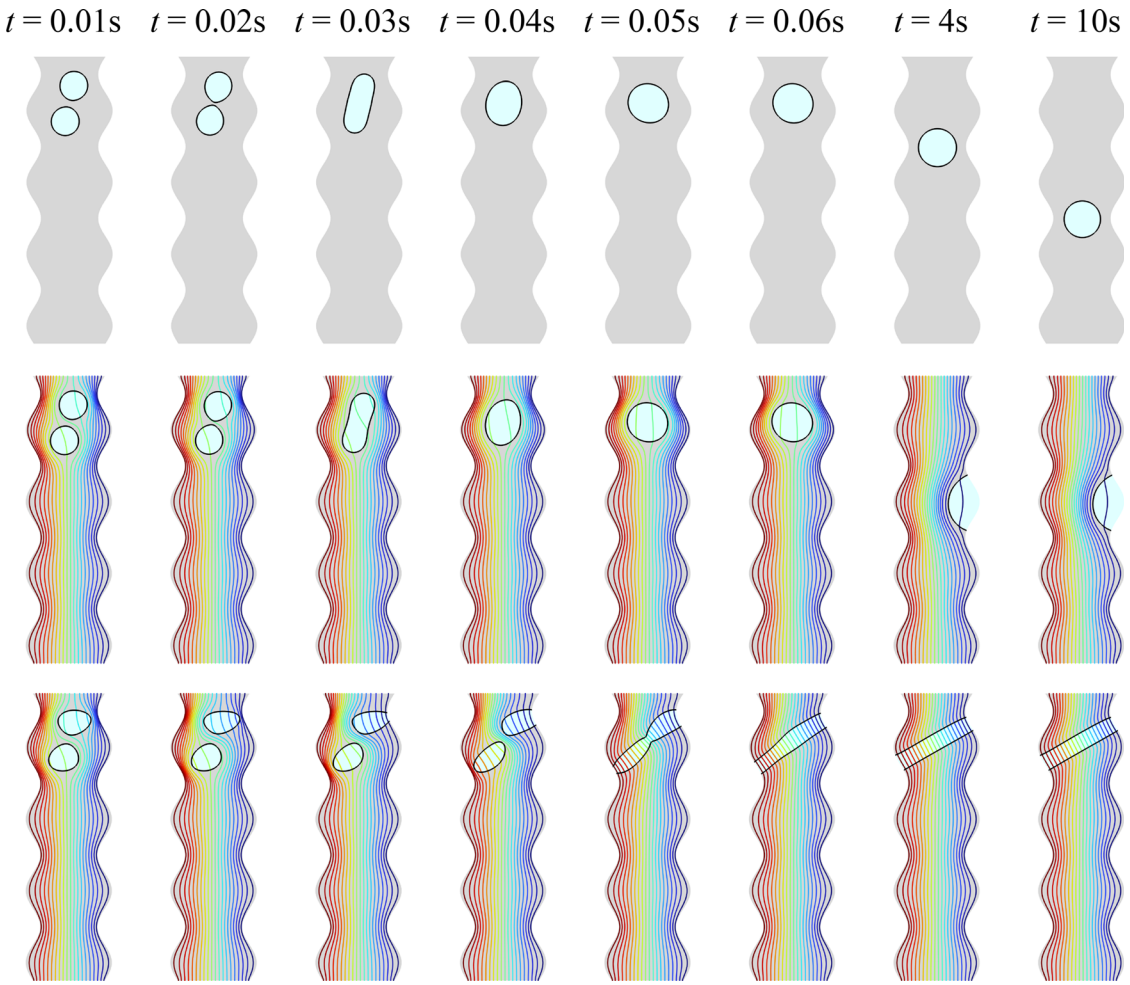

FIG. 11. Electric potential distribution and the motion of the droplets at $A = 0.5$ and $L = 5$ for different V_0: first row: $V_0 = 0$; second row: $V_0 = 500$ V; third row: $V_0 = 2000$ V.

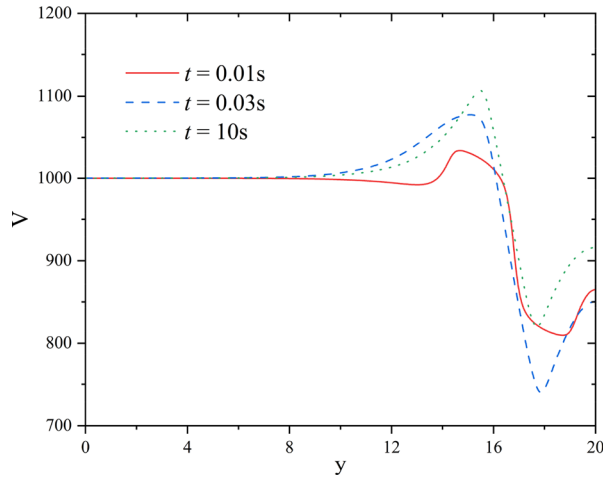

FIG. 12. Electric potential curve along the center axis in the case at $A = 0.5$ and $L = 5$ for $V_0 = 2000$ V.

y-coordinate of the droplet position at $t = 10$s gradually increases. In other words, as A increases, the influence on the droplet descent becomes greater, causing the droplet to descend more slowly. Specifically, when $A = 0.75$, the wall is closer to the initial position of the droplet. At $t = 10$s, the droplet hardly descends and instead adheres around $y = 16$.

Figure 15 illustrates the impact of different A values on the electric potential distribution along the vertical center axis. Based on the analysis of Fig. 14, it is evident that the potential gradient is minimized on the surface of the droplet, resulting in a larger gradient near its edges. The peak potential values correspond to the locations of the droplet. Specifically, when $A = 0.25$, the potential trough is observed around $y = 6$. As seen in Figs. 8(a) and 14, it is apparent that the droplet is positioned close to the right wall of the channel, precisely around $y = 6$. However, at $A = 0.75$, the peak potential along the central axis is found near $y = 16$, again aligning with the location of droplet. In other words, for the wavy wall, the locations of the peaks rise with an increase in A. As shown in Fig. 14, when A increases, the amplitude of the wall waves increases, causing droplets to be adsorbed onto the wall earlier. Consequently, the y-coordinate corresponding to the peak

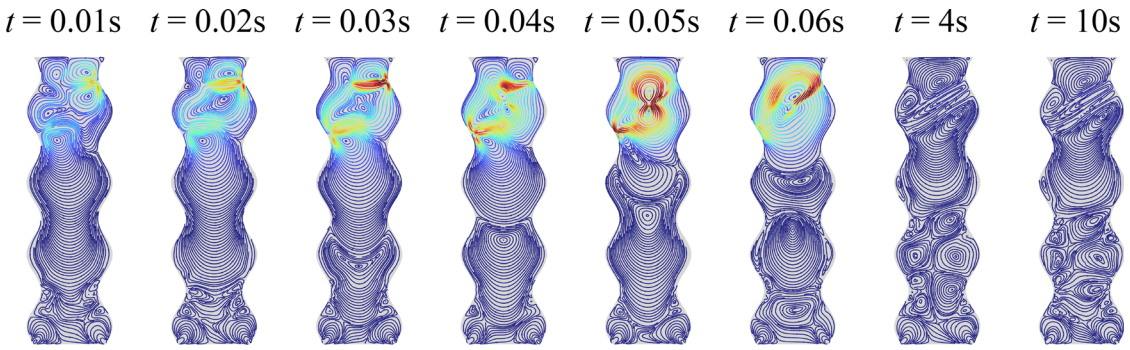

FIG. 13. Streamlines of the case at $A = 0.5$ and $L = 5$ for $V_0 = 2000$ V.

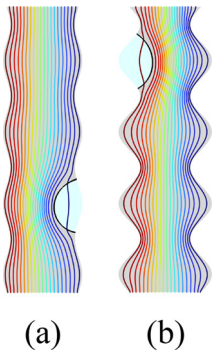

FIG. 14. Electric potential distribution and the motion of the droplets at $V_0 = 500$ V, $t = 10$s, $L = 5$, (a) $A = 0.25$, (b) $A = 0.75$.

position of the electric potential along the central axis becomes larger. It is important to note that at this position, the potential exhibits a peak rather than a trough due to the droplet being situated near the left wall of the channel.

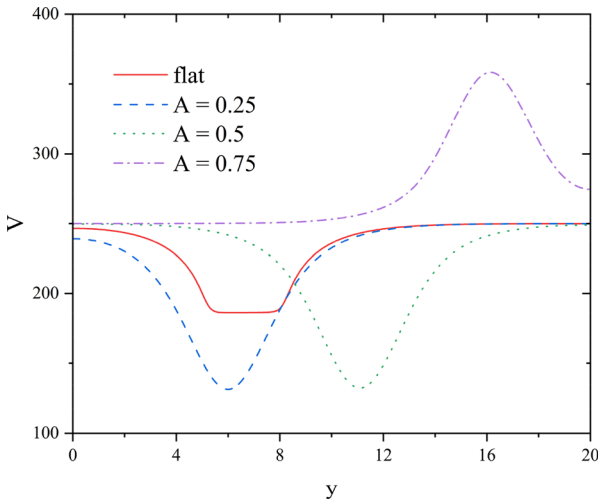

FIG. 15. Electric potential curve along the center axis at $V_0 = 500$ V, $L = 5$, $t = 10$s.

D. Effect of L

Figure 16 shows the impact of wavy wall wavelength on the droplet position and electric potential distribution. It can be seen that at $t = 10$s, the droplets tend to reside at the locations where the wall protrudes outward. Similar to the effect of wavy wall amplitude, as L increases, the y-coordinate of the droplet at $t = 10$s decreases. In other words, a decrease in L inhibits the descent of the droplet.

Figure 17 presents electric potential curve along the center axis at $A = 0.5$, $V_0 = 500$ V, and $t = 10$s. The peaks in the electric potential curve correspond to the positions of the droplets. As L decreases, the y-coordinates corresponding to the peaks increase, and the peak value also rises. In fact, as L decreases, the changes in wall shape cause the droplet to increase in size along the x-direction at $t = 10$s, leading to an increase in the electric potential gradient at the outer edges of the droplet.

V. CONCLUSION

The present study proposed a study on the effects of wavy walls and electric fields on the deformation and coalescence of droplets. Based on the COMSOL, a fully coupled model was developed incorporating the Navier–Stokes equations, Maxwell stress tensor, and phase-field model. The effects of the applied electric field strength, wavy wall amplitude, and wavy wall wavelength are investigated. The simulations reveal that for the cavity with flat walls, in the absence of an applied electric field, the two droplets coalesce and descend. When the electric

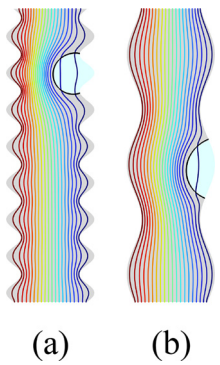

FIG. 16. Electric potential distribution and the motion of the droplets at $A = 0.5$, $V_0 = 500$ V, $t = 10$s. (a) $L = 2.5$ and (b) $L = 7.5$.

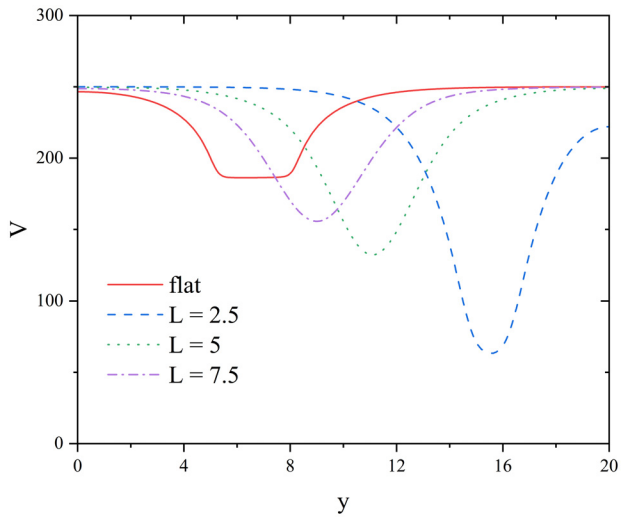

FIG. 17. Electric potential curve along the center axis at $A = 0.5$, $V_0 = 500$ V, $t = 10$s.

field strength is low, the descent of the droplets is affected, causing them to adhere to one sidewall. When the potential is increased to 2000 V, the droplets coalesce and form a barrier layer, dividing the cavity into upper and lower sections. This barrier layer remains stationary and does not descend. Additionally, the influence of wavy walls is significant and at $A = 0.5$, $L = 5$ and 2000 V, resulting in the formation of an inclined barrier layer. As A increases, the influence of wall on the droplet descent becomes greater, causing the droplet to descend more slowly. Conversely, as L decreases, the descent of the droplet is inhibited.

Although the present study employs a two-dimensional approach, which provides a robust and accurate representation, it is essential to acknowledge that three-dimensional numerical simulations more closely mirror real-world conditions. Therefore, extending this work to three dimensions is crucial, as it can offer deeper insights, particularly in capturing the full complexity of droplet interactions under the influence of electric fields and wavy walls. Furthermore, it remains crucial to examine the behavior of various liquid types under analogous conditions, in order to fully appreciate the broad spectrum of potential applications afforded by this phenomenon.

AUTHOR DECLARATIONS

Conflict of Interest

The authors have no conflicts to disclose.

Author Contributions

Yuan Ma: Conceptualization (equal); Funding acquisition (equal); Resources (equal); Validation (equal); Writing – original draft (equal). **Rasul Mohebbi:** Formal analysis (equal); Investigation (equal); Supervision (equal); Writing – review & editing (equal). **Zhi-gang Yang:** Project administration (equal).

DATA AVAILABILITY

The data that support the findings of this study are available from the corresponding author upon reasonable request.

REFERENCES

[1]T. M. Ho, A. Razzaghi, A. Ramachandran, and K. S. Mikkonen, "Emulsion characterization via microfluidic devices: A review on interfacial tension and stability to coalescence," Adv. Colloid Interface Sci. **299**, 102541 (2022).
[2]J. Kamp, J. Villwock, and M. Kraume, "Drop coalescence in technical liquid/liquid applications: A review on experimental techniques and modeling approaches," Rev. Chem. Eng. **33**(1), 1–47 (2017).
[3]J. S. Eow and M. Ghadiri, "Electrostatic enhancement of coalescence of water droplets in oil: A review of the technology," Chem. Eng. J. **85**(2–3), 357–368 (2002).
[4]J. Snoeijer, J. E. Sprittles, and J. H. Eggers, "Coalescence dynamics," Annu. Rev. Fluid Mech. **57**, 61–87 (2025).
[5]D. Seo, S. Oh, B. Moon, H. Kim, J. Kim, C. Lee, and Y. Nam, "Influence of lubricant-mediated droplet coalescence on frosting delay on lubricant impregnated surfaces," Int. J. Heat Mass Transfer **128**, 217–228 (2019).
[6]H. Zaman, N. Ali, C. Zhou, A. Khan, F. Ali, C. T. Tian, and M. Bilal, "Magnetically recoverable poly (methyl methacrylate-acrylic acid)/iron oxide magnetic composites nanomaterials with hydrophilic wettability for efficient oil-water separation," J. Environ. Manage. **319**, 115690 (2022).
[7]R. Roy, R. L. Seiler, J. A. Weibel, and S. V. Garimella, "Droplets on soft surfaces exhibit a reluctance to coalesce due to an intervening wetting ridge," Adv. Mater. Inter. **7**(17), 2000731 (2020).
[8]J. S. Sander, R. M. Erb, L. Li, A. Gurijala, and Y. M. Chiang, "High-performance battery electrodes via magnetic templating," Nat. Energy **1**(8), 1–7 (2016).
[9]N. L. Gluchowski, M. Becuwe, T. C. Walther, and R. V. Farese, "Lipid droplets and liver disease: From basic biology to clinical implications," Nat. Rev. Gastroenterol. Hepatol. **14**(6), 343–355 (2017).
[10]A. Hadidi and D. Jalali-Vahid, "Numerical simulation of dielectric bubbles coalescence under the effects of uniform magnetic field," Theor. Comput. Fluid Dyn. **30**, 165–184 (2016).
[11]E. Hemachandran, T. Laurell, and A. K. Sen, "Continuous droplet coalescence in a microchannel coflow using bulk acoustic waves," Phys. Rev. Appl. **12**(4), 044008 (2019).
[12]S. Roy and R. M. Thaokar, "Numerical study of coalescence and non-coalescence of two conducting drops in a non-conducting medium under electric field," J. Electrostat. **108**, 103515 (2020).
[13]A. Ghaffari, S. H. Hashemabadi, and M. Bazmi, "CFD simulation of equilibrium shape and coalescence of ferrofluid droplets subjected to uniform magnetic field," Colloids Surf, A **481**, 186–198 (2015).
[14]M. R. Hassan, J. Zhang, and C. Wang, "Digital microfluidics: Magnetic transportation and coalescence of sessile droplets on hydrophobic surfaces," Langmuir. **37**(19), 5823–5837 (2021).
[15]A. Shams Taleghani and M. Sheikholeslam Noori, "Numerical investigation of coalescence phenomena, affected by surface acoustic waves," Eur. Phys. J. Plus **137**(8), 975 (2022).
[16]I. Adeyemi, M. Meribout, L. Khezzar, N. Kharoua, and K. AlHammadi, "Numerical assessment of ultrasound supported coalescence of water droplets in crude oil," Ultrason. Sonochem. **88**, 106085 (2022).
[17]X. Huang, L. He, X. Luo, H. Yin, and D. Yang, "Deformation and coalescence of water droplets in viscous fluid under a direct current electric field," Int. J. Multiphase Flow **118**, 1–9 (2019).
[18]M. R. Mardani, D. D. Ganji, and K. H. Hosseinzadeh, "Numerical investigation of droplet coalescence of saltwater in the crude oil by external electric field," J. Mol. Liq. **346**, 117111 (2022).
[19]B. Li, Z. Wang, V. Vivacqua, M. Ghadiri, J. Wang, W. Zhang, D. Wang, H. Liu, Z. Sun, and Z. Wang, "Drop-interface electrocoalescence mode transition under a direct current electric field," Chem. Eng. Sci. **213**, 115360 (2020).
[20]S. Luo, J. Schiffbauer, and T. Luo, "Effect of electric field non-uniformity on droplets coalescence," Phys. Chem. Chem. Phys. **18**(43), 29786–29796 (2016).
[21]H. Hadidi, R. Kamali, and M. K. Manshadi, "Numerical simulation of a novel non-uniform electric field design to enhance the electrocoalescence of droplets," Eur. J. Mech.-B/Fluids **80**, 206–215 (2020).
[22]S. H. Mousavi, M. Ghadiri, and M. Buckley, "Electro-coalescence of water drops in oils under pulsatile electric fields," Chem. Eng. Sci. **120**, 130–142 (2014).

[23]Y. Sun, D. Yang, H. Sun, H. Wu, Q. Chang, L. Shi, Y. Cao, Y. He, and T. Xie, "Experimental study on the falling and coalescence characteristics of droplets under alternating electric fields," Colloids Surf, A **603**, 125136 (2020).
[24]Z. Sun, Z. Qi, N. Li, Y. Jiang, R. Ren, B. Li, and Z. Wang, "Numerical analysis on drop-drop electrocoalescence behavior under different electric field parameters," Sep. Sci. Technol. **57**(13), 2099–2115 (2022).
[25]G. Emmi and M. Bottarelli, "Enhancement of shallow ground heat exchanger with phase change material," Renewable Energy **206**, 828–837 (2023).
[26]S. Sheikhi and M. R. Flynn, "Porous media gravity current flow over an inter-bed layer: The impact of dispersion and distributed drainage," J. Fluid Mech. **984**, A33 (2024).
[27]J. Klostermann, K. Schaake, and R. Schwarze, "Numerical simulation of a single rising bubble by VOF with surface compression," Int. J. Numer. Methods Fluids **71**(8), 960–982 (2013).
[28]H. A. Sormoli, A. Mojra, and G. Heidarinejad, "A novel gas embolotherapy using microbubbles electrocoalescence for cancer treatment," Comput. Methods Programs Biomed. **244**, 107953 (2024).
[29]G. S. Goh, M. D. Goodwin, J. F. Huang, H. Kavnoudias, and A. Holden, "A pilot first-in-human study of embrace, a polyethylene glycol-based liquid embolic agent, in the embolization of malignant and benign hypervascular tumors," J. Vasc. Interventional Radiol. **33**(6), 660–667 (2022).